Cartilage Thickness: Factors Influencing Multidetector CT Measurements in a Phantom Study[1]

Andrew E. Anderson, BS
Benjamin J. Ellis, BS
Christopher L. Peters, MD
Jeffrey A. Weiss, PhD

Purpose: To prospectively assess in a phantom the reconstruction errors and detection limits of cartilage thickness measurements obtained with multidetector computed tomographic (CT) arthrography, as a function of contrast agent concentration, scanning direction, spatial resolution, joint spacing, and tube current, with known measurements as the reference standard.

Materials and Methods: A phantom with nine chambers was constructed. Each chamber had a nylon cylinder encased by sleeves of aluminum and polycarbonate to simulate trabecular bone, cortical bone, and cartilage. Varying simulated cartilage thicknesses and 10 joint space widths were assessed. On 3 days, the phantom was scanned with and without contrast agent administration and with the chamber axes both perpendicular and parallel to the scanner axis. Images were reconstructed at 1.0- and 0.5-mm intervals. Contrast agent concentration and tube current were varied. The simulated cartilage thickness was determined by using image segmentation. Root mean squared errors and mean residual errors were used to characterize the measurements. The reproducibility of the CT scanner and image segmentation results was determined.

Results: Simulated cartilage greater than 1.0 mm in thickness was reconstructed with less than 10% error when either no contrast agent or a low concentration (25%) of contrast agent was used. Error increased as contrast agent concentration increased. Decreasing the simulated joint space width to 0.5 mm caused slight increases in error; however, error increased substantially at joint spaces narrower than 0.5 mm. Errors in measurements derived from anisotropic CT data were greater than errors in measurements derived from isotropic data. Altering the tube current did not substantially affect reconstruction errors.

Conclusion: The study revealed lower boundaries and the repeatability of simulated cartilage thickness measurements obtained by using multidetector CT arthrography and yielded data pertinent to choosing the contrast agent concentration, joint space width, scanning direction, and spatial resolution to reduce reconstruction errors.

[1] From the Department of Bioengineering and Scientific Computing and Imaging Institute (A.E.A., B.J.E., J.A.W.); and Department of Orthopedics (C.L.P., J.A.W.), University of Utah, 72 S Central Campus Dr, Room 2646, Salt Lake City, UT 84112. Received December 26, 2006; revision requested March 1, 2007; revision received April 23; accepted May 25; final version accepted July 9. Supported by the Orthopaedic Research and Education Foundation. **Address correspondence to** J.A.W. (e-mail: *jeff.weiss@utah.edu*).

Evidence suggests that multidetector computed tomographic (CT) arthrography may be more sensitive than magnetic resonance (MR) imaging for depicting cartilaginous lesions (1–5) and quantifying cartilage thickness (6). However, fat-suppressed spoiled gradient-recalled acquisition in the steady state is still considered the best protocol for imaging articular cartilage (7–16). Although a substantial body of research (17–22) has been performed to examine MR cartilage reconstruction errors, less attention has been given to CT arthrography (6,18,23). Nevertheless, MR data–derived estimates of cartilage thickness are often validated by means of direct comparison with CT arthrography results (18,19); this protocol might erroneously imply that CT arthrography is the reference standard for such estimations.

Examinations performed to compare cartilage thickness measurements estimated from CT arthrography data with measurements obtained from physical examinations of anatomic sections generally have been qualitative assessments (18,23). To our knowledge, in only one study have quantitative cartilage thickness measurements been compared between reconstructed multidetector CT arthrograms and excised tissue samples (6). However, the use of harvested cartilage plugs in that study limited the range of cartilage thicknesses that could be analyzed.

Evidence suggests that cartilage may actually swell during the early stages of osteoarthritis (24). Therefore, it would be useful to quantify cartilage thickness by using CT arthrography in patients who report having pain that may be related to osteoarthritis but do not have direct radiographic evidence of thinning or localized defects. In terms of experimental investigations of cartilage contact mechanics performed by using cadaveric tissue, the quantification of differences in reconstruction errors between standard CT and CT arthrography would help to clarify whether cadaveric joints should be completely dissected and imaged with air or the joint capsule should be left intact.

The boundaries of cartilage thickness detection—and hence the ultimate reconstruction error—with multidetector CT arthrography remain unknown. In addition, to our knowledge, the influence of imaging parameters on the ability to detect and reconstruct articular cartilage from multidetector CT arthrography data had not been assessed. Thus, the purpose of our study was to prospectively assess in a phantom the reconstruction errors and detection limits of cartilage thickness measurements obtained with multidetector CT arthrography, as a function of contrast agent concentration, scanning direction, spatial resolution, joint spacing, and tube current, with known measurements as the reference standard.

Advances in Knowledge

- Changing the contrast agent concentration, scanning direction, and/or spatial resolution had the greatest effect on simulated cartilage reconstruction errors; altering the joint spacing and tube current resulted in minor changes.
- The results of our study establish lower boundaries and the repeatability of cartilage thickness measurements with multidetector CT.

Materials and Methods

Phantom Description

An imaging phantom to quantify the error in reconstructing cartilage thickness was designed and manufactured (CNA Precision Machine, Ogden, Utah) (Fig 1). The phantom body was constructed of nylon (Natural Cast Nylon; Professional Plastics, Fullerton, Calif). Nine chambers were drilled into the phantom body (Fig 1). Each chamber was composed of a central nylon cylinder encased by cylindric sleeves of aluminum and polycarbonate (Standard Polycarbonate; Professional Plastics). The central nylon cylinder simulated trabecular bone; the cylindric sleeve of aluminum, cortical bone; and the outer cylindric sleeve of polycarbonate, cartilage (Fig 1b). All aluminum cylinders were manufactured to a wall thickness of 1.00 mm to represent cortical bone with a constant thickness. The polycarbonate cylindric sleeves were manufactured to wall thicknesses of 0.25, 0.50, 0.75, 1.00, 2.00, and 4.00 mm (Fig 1a, phantom chambers *1–6*). An outer polycarbonate four-prong spacer was press fit into each chamber between the outer layer of simulated cartilage and the adjacent nylon phantom body (Fig 1b). The spacer held the central cylinders securely in place and provided a joint space that could be filled with contrast agent. The joint space width in phantom chambers *1–6* (Fig 1a) was held constant at 2.0 mm. Varying joint space widths (0.25, 0.50, and 1.00 mm) were used with a constant simulated cartilage thickness of 2.00 mm in the remaining three compartments (Fig 1a, phantom chambers *7–9*). Finally, nylon-threaded caps were used to seal the fluid inside the chambers. The manufacturer used a micrometer with an accuracy of ±0.01 mm to determine the wall thickness tolerance of the aluminum and polycarbonate cylindric sleeves, representing cortical bone and cartilage, respectively.

Implication for Patient Care

- Careful consideration of the contrast agent concentration, scanning direction, and spatial resolution may reduce errors when reconstructing cartilage with use of the patient's multidetector CT arthrography data.

Published online
10.1148/radiol.2461062192

Radiology 2008; 246:133–141

Abbreviation:
RMS = root mean squared

Author contributions:
Guarantor of integrity of entire study, J.A.W.; study concepts/study design or data acquisition or data analysis/interpretation, all authors; manuscript drafting or manuscript revision for important intellectual content, all authors; manuscript final version approval, all authors; literature research, all authors; experimental studies, all authors; statistical analysis, A.E.A., J.A.W.; and manuscript editing, all authors

Authors stated no financial relationship to disclose.

The tolerance was reported to be within ±0.07 mm.

Nylon, polycarbonate, and aluminum were chosen as phantom materials because they have x-ray attenuation values similar to those of trabecular bone, cartilage, and cortical bone, respectively (25–28). The size of the phantom (250 × 250 mm) was representative of a typical field of view used to image diarthrodial joints in humans. The outer diameter of each compartment—that is, the outer boundary of simulated cartilage—was kept constant at 52 mm, while the diameters of the aluminum sleeve and central nylon cylinder were adjusted to between 38 and 46 mm to accommodate differences in cartilage thickness and joint spacing. This range of cylinder diameters is similar to that for femoral and humeral heads in humans reported in the literature (29–31). The range of cartilage thicknesses (0.25–4.00 mm) was chosen to represent the range of articular cartilage thicknesses in humans reported in the literature (32,33).

CT Protocol

All CT examinations of phantoms were performed with a Somatom Sensation 64 scanner (Siemens Medical Solutions, Malvern, Pa). This scanner makes use of the periodic motion of the focal spot in the longitudinal direction to double the number of simultaneously acquired sections, with the goals of improving spatial resolution and eliminating spiral artifacts, regardless of spiral pitch. The following scanning parameters were kept constant: 120 kVp, 512 × 512 matrix, 300-mm field of view, and 1-mm section thickness. Six contrast material–enhanced CT examinations and four nonenhanced examinations were performed. The imaging protocol detailed below was performed on three separate days to assess the reproducibility of the CT scanner and segmentation procedure results.

Contrast-enhanced CT.—Iohexol (350 mg of iodine per milliliter) (Omnipaque 350; GE Healthcare, Princeton, NJ) was mixed with 1% lidocaine hydrochloride (Hospira, Lake Forest, Ill) in separate concentrations of 25%, 50%, and 75%. The phantom was scanned by using a tube current of 200 mAs for each of the three concentrations (three examinations) in the transverse or frontal plane (Fig 1a). The laser guide was used to align the CT section axis perpendicular to the phantom chambers' longitudinal axes and thereby minimize volumetric averaging between sections. Two additional transverse examinations were conducted by using tube currents of 150 and 250 mAs with the phantom filled with a 50% concentration of the contrast agent. To intentionally introduce volumetric averaging, an examination of the phantom filled with a 50% contrast agent concentration was performed parallel to the phantom chambers' longitudinal axis using a tube current of 200 mAs (Fig 1a).

Nonenhanced CT.—To estimate the error in cartilage thickness reconstruc-

Figure 1

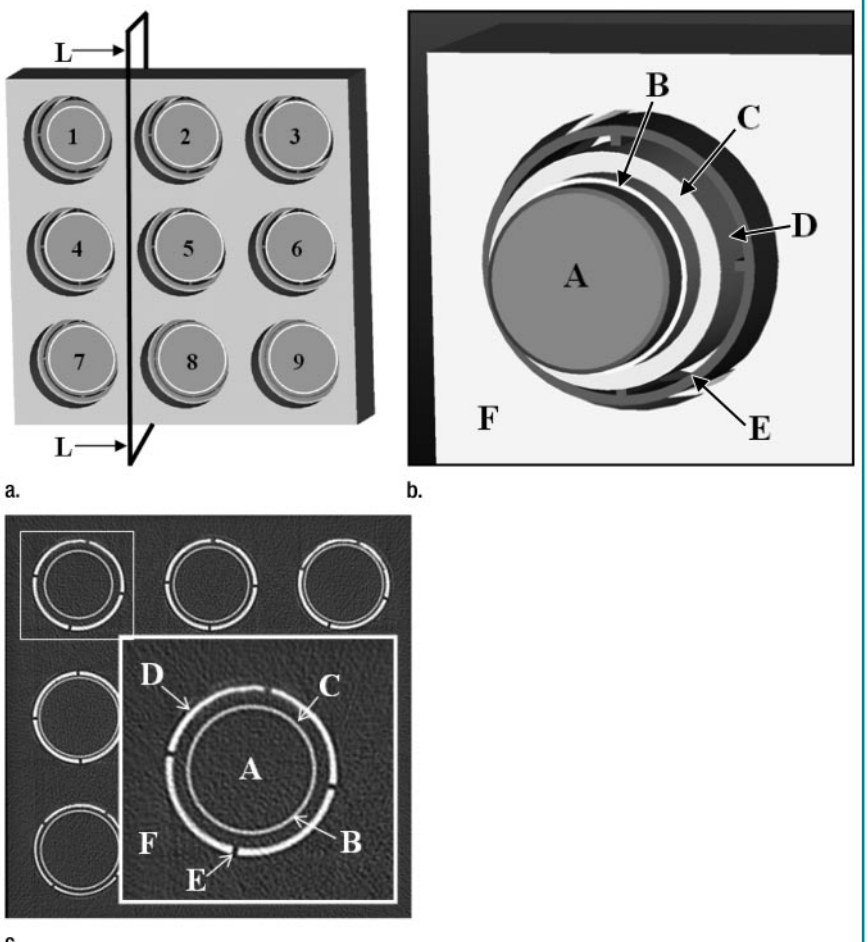

Figure 1: **(a)** Schematic illustration of phantom used to assess detection limits of transverse multidetector CT. The longitudinal imaging plane *(L)* is also shown. Simulated cartilage thicknesses of 4.00, 2.00, 1.00, 0.75, 0.50, and 0.25 mm were used with a constant joint space width of 2.0 mm in chambers *1–6*, respectively. A constant cartilage thickness of 2.0 mm was used with joint space widths of 1.00, 0.50, and 0.25 mm in chambers *7–9*, respectively. **(b)** Expanded view of chamber 1 shows nylon cylinder center *(A)* representing trabecular bone, 1-mm-thick aluminum sleeve *(B)* representing cortical bone, polycarbonate sleeve *(C)* representing cartilage, joint space *(D)*, polycarbonate four-pronged spacer *(E)* used to create joint space, and bulk of phantom body *(F)* constructed of nylon. **(c)** CT scan of phantom filled with contrast agent; inset shows image details of chamber 1; letters correspond to those in **b**.

tion for disarticulated dissected cadaveric joints, the phantom was imaged when it was not filled with contrast agent. Three nonenhanced examinations were performed in the transverse plane by using tube currents of 150, 200, and 250 mAs. To intentionally introduce volumetric averaging between successive sections, a final nonenhanced CT examination was performed parallel to the phantom chambers' longitudinal axis using a tube current of 200 mAs.

Image Segmentation, Surface Reconstruction, and Thickness Measurement

Phantom image data were transferred to a Linux workstation (Universal Systems, Salt Lake City, Utah) for postprocessing. To assess differences in reconstruction errors between anisotropic (0.586 × 1.0 × 0.586 mm) and near-isotropic (0.586 × 0.5 × 0.586 mm) spatial resolution, image data were resampled after the CT examination by using 0.5-mm section intervals for the contrast-enhanced and nonenhanced longitudinal examinations. The use of inner postscanning reconstructions in the transverse plane would have been ambiguous since the curvature of the phantom chambers did not change as sections were imaged in this direction.

Separate splines for the outer surface of the aluminum cylinder (representing cortical bone) and the boundary between the polycarbonate cylinder (representing outer layer of simulated cartilage) and either air (nonenhanced examination) or contrast agent (contrast-enhanced examination) were extracted from the image data. Both automatic and semiautomatic thresholding techniques were applied by using commercial segmentation software (Amira 4.1; Mercury Computer Systems, Chelmsford, Mass).

Each data set was automatically thresholded by using a masking technique available in the segmentation software, which allows the user to highlight pixels over a range of defined attenuation values. For data sets with contrast agent included, the mask was adjusted incrementally until all pixels representing nylon (the bulk of the phantom body) were excluded. Thus, pixels with attenuation values greater than this masked range were defined as contrast agent and simulated cortical bone, whereas those with attenuation values less than this masked range were defined as simulated cartilage. For the nonenhanced CT data sets, the same masking procedure was used to define the simulated cortical bone boundary; however, the boundary between simulated cartilage and air was defined by reversing the mask such that all pixels representing the nylon body of the phantom were included. As mentioned above, the masking procedure was performed for each CT data set separately to ensure that the appropriate threshold range was chosen independently of alterations in tube current, contrast agent concentration, spatial resolution, or scanning direction. After all data sets were masked, it was later determined that interscan threshold values varied by less than 5%.

Owing to CT volumetric averaging, it was necessary to use a semiautomatic thresholding technique for the data sets in which contrast agent was included. However, this procedure was only required for phantom chambers with simulated cartilage thicknesses of 0.50 and 0.25 mm (Fig 1a, chambers *5* and *6*). Simulated cartilage with thicknesses greater than these was effectively segmented by using the automatic method, regardless of contrast agent concentration, tube current, spatial resolution, or scanning direction. For the 0.50- and 0.25-mm chambers, first the baseline automatic threshold value was used to define a general segmentation spline. Next, regions where pixels blended together were separated by using a paintbrush tool available in the segmentation software such that the resulting spline followed the general boundary between simulated cartilage and contrast agent. Although volumetric averaging occurred, the attenuation gradient between contrast agent and simulated cartilage was strong enough to allow easy visual separation. To ensure uniformity, all of the semiautomatic segmentations were performed by the senior author (A.E.A.).

Splines were stacked on top of one another and triangulated by using the marching cubes algorithm (34) to form surfaces that represented the outer surfaces of simulated cortical bone and cartilage. To preserve the native splines of the CT image data, the resulting polygonal surfaces were not altered by means of decimation or smoothing. A published algorithm was used to assign a thickness to each of the nodes that defined the simulated cartilage surface (35). This algorithm has been tested for accuracy by using concentric cylinders with known thicknesses. Reported errors were less than 2% (35).

Error Analysis

Thickness values were analyzed to determine the reconstruction errors and detection limits of multidetector CT and to investigate the influences of tube current, joint spacing, contrast agent concentration, and scanning direction. The overall thickness error for each phantom chamber measurement was assessed by using the root mean squared (RMS) error (E_{RMS}) criteria:

$$E_{RMS} = \left[\sum_{i=1}^{n} (t_i^{CT} - t^{Phan})^2 \Big/ n \right]^{1/2}, \qquad (1)$$

where the summation (Σ) is over the number of surface nodes *(n)* from $i = 1$ to n, t_i^{CT} is the thickness of the ith node of the reconstructed surface, and t^{Phan} is the constant thickness assessed by means of direct manufacturer measurement of the phantom. The mean residual error (MRE) was calculated as follows to determine the direction of the error:

$$MRE = \left[\sum_{i=1}^{n} (t_i^{CT} - t^{Phan}) \right] \Big/ n. \qquad (2)$$

Statistical Analyses

Descriptive statistics were calculated by using statistical software (SPSS 11.5 for Windows 2002; SPSS, Chicago, Ill). Specifically, RMS errors and mean residual errors were averaged for the 3 days on which the CT exami-

nations were conducted. The resulting mean values, with corresponding standard deviation error bars, were plotted (SigmaPlot 8.0; Systat Software, San Jose, Calif) to determine the interscan variation in reconstruction error.

Results

Contrast-enhanced CT

There were notable differences in average RMS error and mean residual error due to alterations in contrast agent concentration (Fig 2). Simulated phantom cartilage thicker than 1.0 mm was reconstructed with less than 10% RMS error and mean residual error when the lowest contrast agent concentration (25%) was used and the direction of CT scanning was transverse to the phantom (Fig

Figure 2

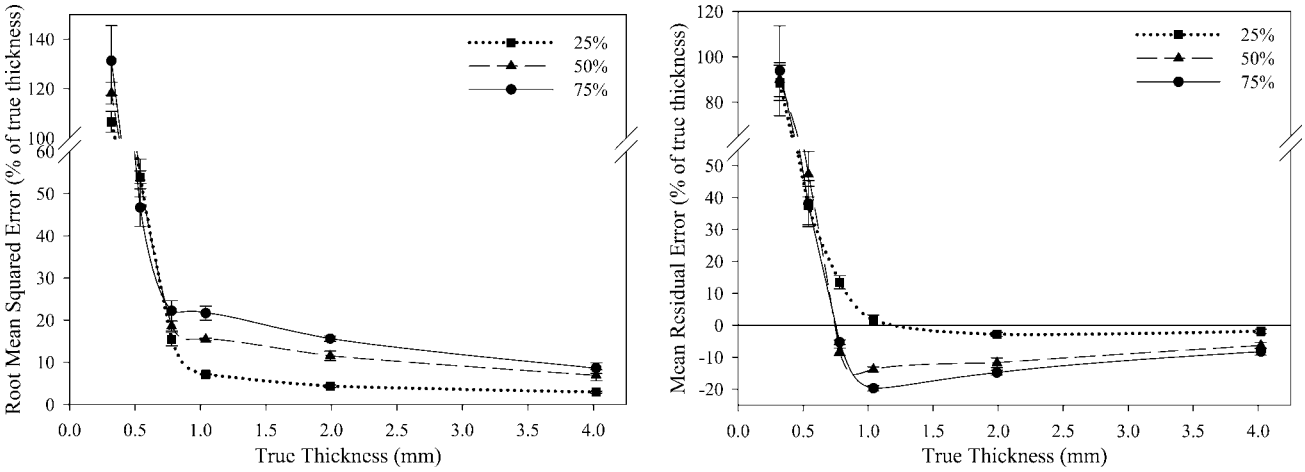

a. b.

Figure 2: Graphs illustrate simulated cartilage **(a)** RMS and **(b)** mean residual reconstruction errors for transverse contrast-enhanced CT data sets, as a function of contrast agent concentration. **(a)** At cartilage thicknesses greater than 0.75 mm, RMS errors increased progressively as the contrast agent concentration increased. Direction of error was dependent on contrast agent concentration and simulated cartilage thickness.

Figure 3

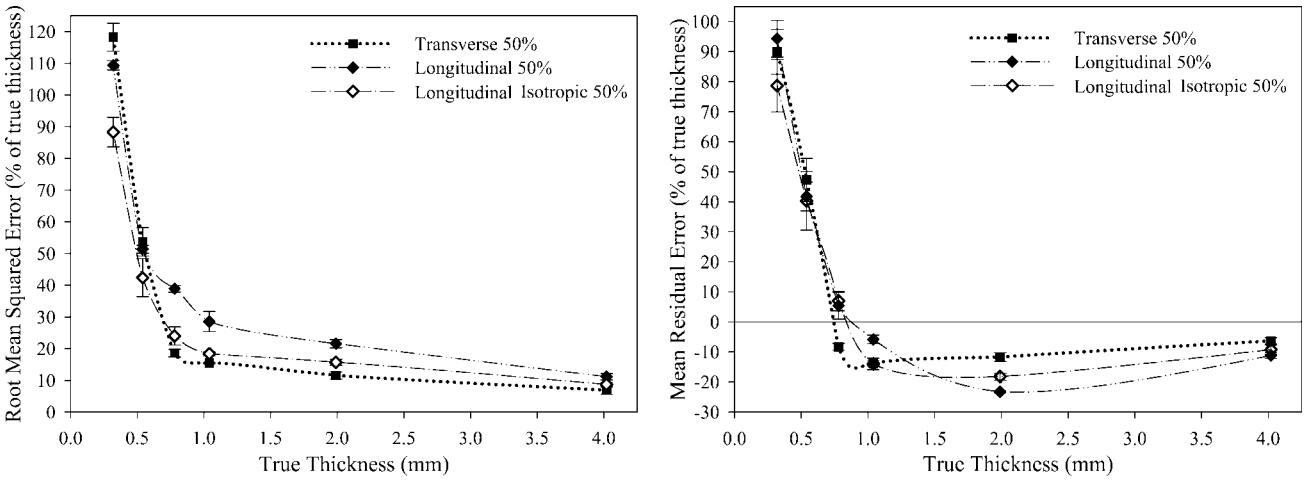

a. b.

Figure 3: Graphs illustrate simulated cartilage **(a)** RMS and **(b)** mean residual reconstruction errors for transverse contrast-enhanced CT data sets obtained with 50% contrast agent concentration, as a function of scanning direction and spatial resolution. Errors were greatest for the anisotropic longitudinal data reconstructions. The isotropic longitudinal reconstructions yielded errors more consistent with transverse CT results.

2). At cartilage thicknesses greater than 0.75 mm, transverse CT–derived RMS reconstruction errors increased progressively as the contrast agent concentration was increased from 25% to 75% (Fig 2a). An increase in contrast agent concentration resulted in a greater tendency for simulated cartilage thicknesses of 1.0–4.0 mm to be underestimated (Fig 2b). However, a shift in error, from underestimation to overestimation, occurred as the cartilage thickness approached the spatial resolution of the image data (0.586 × 0.586 mm) (Fig 2b).

Substantial differences in average reconstruction errors were also noted when the scanning direction and spatial resolution were altered (Fig 3). For simulated cartilage thicker than 1.0 mm (Fig 3), anisotropic longitudinal reconstructions at the 50% contrast agent concentration yielded greater RMS and mean residual errors than did the corresponding transverse and near-isotropic longitudinal reconstructions at the 50% concentration. Finally, altering the tube current resulted in negligible differences over the range of simulated cartilage thicknesses analyzed (data not shown).

There were differences in RMS errors over the range of joint space widths assessed due to changes in contrast agent concentration and scanning direction (Fig 4) but no marked differences due to alterations in tube current (data not shown). Errors increased as the contrast agent concentration was increased (Fig 4). For each transverse CT measurement, RMS errors increased slightly when the joint space width was decreased from 2.0 to 0.5 mm; at widths lower than 0.5 mm, however, errors increased substantially (Fig 4). The anisotropic longitudinal CT data set (1.0-mm thickness reconstruction) yielded greater RMS errors than did the corresponding transverse and near-isotropic longitudinal data sets (0.5-mm thickness reconstruction) over the full range of joint space widths analyzed (Fig 4). Mean residual error analysis revealed that simulated cartilage thickness was underestimated in all data sets and that these errors were the smallest with transverse 25%-concentration CT scanning (data not shown).

Examination of the standard deviation error bars in Figures 2–4 revealed high levels of reproducibility for measurements of 0.75–4.00-mm-thick simulated cartilage. In addition, the standard deviation error bars and adjacent results within this range did not overlap. For measurements of 0.25–0.50-mm-thick simulated cartilage, standard deviations were much larger and error bars and adjacent data points overlapped.

Nonenhanced CT

Reconstructions of nonenhanced transverse CT data at 200 mAs resulted in RMS errors of less than 10% for measurements of cartilage thicker than 1.0 mm (Fig 5a). RMS errors in the nonenhanced CT data were within 2% of those reported for transverse contrast-enhanced scanning of 0.75–4.00-mm-thick simulated cartilage at the 25% contrast agent concentration. RMS errors in measurements of simulated cartilage less than 1.0 mm thick increased substantially, but they leveled out at thicknesses of 0.50–0.25 mm (Fig 5a). The leveling point on the RMS plot aligned well with corresponding points of inflection on the mean residual error plot (Fig 5b). Therefore, the lack of increase in RMS error at a thickness of 0.25 mm was due to a shift from underestimation to overestimation of cartilage thickness. RMS errors in the longitudinal and near-isotropic longitudinal data sets were similar to errors in the transverse measurements of 2.0- and 4.0-mm-thick simulated cartilage; however, errors increased substantially at thicknesses of less than 2.0 mm (Fig 5a). Errors in longitudinal anisotropic CT measurements were substantially greater than errors in transverse and near-isotropic longitudinal CT measurements of simulated cartilage less than 2.0 mm thick (Fig 5a). Altering the tube current from 150 to 250 mAs did not have an appreciable effect on RMS or mean residual errors in the transverse plane (data not shown).

Like the standard deviation error bars for contrast-enhanced CT scanning, the standard deviation error bars for nonenhanced scanning were negligible for measurements of the thicker (0.75–4.00 mm) simulated cartilage, but they were larger when the thickness was decreased to below this range. In addition, standard deviation error bars did not overlap with adjacent data points within this thickness range, but they did at cartilage thicknesses of less than 0.75 mm.

Figure 4

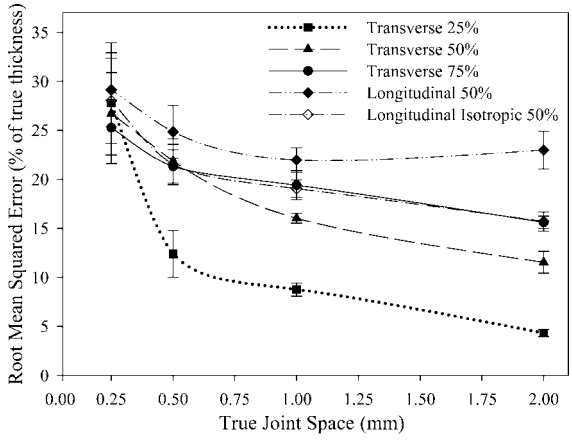

Figure 4: Graph illustrates simulated cartilage RMS errors as a function of joint space width, contrast agent concentration, scanning direction, and spatial resolution. Errors increased as contrast agent concentration increased. There were fewer reconstruction errors in the isotropic longitudinal data set than in the anisotropic data set in the same imaging plane.

Discussion

To our knowledge, our study is the first in which the detection limits of multidetector CT were quantified by using a phantom. Simulated cartilage thicker than 1.0 mm was reconstructed with less than 10% RMS and mean residual

Figure 5

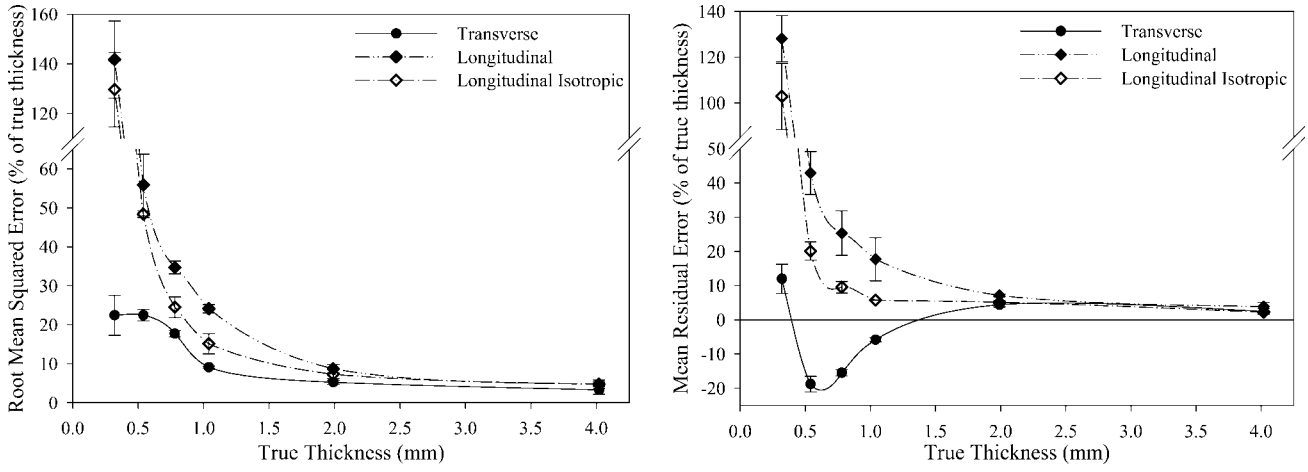

Figure 5: Graphs illustrate simulated cartilage **(a)** RMS and **(b)** mean residual reconstruction errors for the nonenhanced CT data sets obtained at 200 mAs, as a function of scanning direction and spatial resolution. There were consistently fewer RMS errors in the isotropic longitudinal data set than in the anisotropic data set for measurements of simulated cartilage less than 2.0 mm thick.

errors when either no contrast agent or a low concentration (25%) of contrast agent was used. Our study results also demonstrate that the CT reconstruction errors were dependent on contrast agent concentration, scanning direction, spatial resolution, and to a lesser extent joint spacing. Alterations in scanner tube current did not substantially affect simulated cartilage thickness reconstruction errors at the thickness ranges tested at both contrast-enhanced and nonenhanced CT.

Care was taken to control confounding factors in our study. The physical thickness of the phantom was measured to a tolerance of ±0.07 mm; thus, variations in the true thickness of the phantom did not have a substantial influence on the perceived phantom thickness measured with CT. In addition, a separate examination was performed whenever a new alteration (eg, in scanning direction, tube voltage, or contrast agent concentration) was applied to isolate specific effects. The entire protocol was repeated on separate days, and only minor interscan variations in measurements of 0.75–4.00-mm-thick simulated cartilage were noted at both contrast-enhanced and nonenhanced scanning. Therefore, within this thickness range, any noted differences in reconstruction error were due to the alteration studied rather than to confounding factors such as CT scanner variability.

The results of the contrast-enhanced CT reconstructions show a direct relationship between contrast agent concentration and reconstruction error. An explanation for this is that as the contrast agent concentration was increased, larger pixel attenuation gradients were established at the boundary between cartilage and contrast agent. This phenomenon initiated more intense volumetric averaging at this boundary and resulted in a greater tendency for cartilage thickness to be underestimated. However, a shift in error, from underestimation to overestimation, occurred as the thickness approached the spatial resolution of the image data (0.586 × 0.586 mm). This shift occurred because the thickness could not decrease much below the width of a single pixel without extensive surface decimation and smoothing. Therefore, although CT has been shown to yield overestimations of the thickness of thin structures (25,26), our study results demonstrate that the direction of the error is dependent on the concentration of fluid in the joint and the spatial resolution of the image data when CT arthrography is used.

El-Khoury et al (6) compared ankle cartilage measurements obtained with double-contrast multidetector CT arthrography and three-dimensional fat-suppressed spoiled gradient-recalled acquisition in the steady state MR imaging with physical measurements of 15 plugs excised from cadaveric ankles (1–2 mm thick); they found that CT was more accurate than MR imaging. Differences in segmentation method, joint geometry, and arthrography technique (use of double vs single contrast agent) between that study and our current investigation make exact comparisons impossible. Nevertheless, the best-fit line of physical plug measurements plotted against multidetector CT estimates in the El-Khoury et al study indicated that cartilage thickness was underestimated by approximately 5% with CT (6), which is consistent with the 25% concentration agent results over the same range of thicknesses in our study.

In terms of limitations, our study results must be interpreted with consideration of the inherent differences between measurements obtained from a phantom and those obtained in experimental studies with real cartilage specimens. It is well known that articular

cartilage exhibits depth- and location-dependent inhomogeneities in material structure (36–38), and these factors were not a part of our study design. In addition, although real tissue and the materials used for our phantom are similar (25–28), they have small differences in x-ray attenuation values. Finally, diarthrodial joints such as the shoulder and hip have spherical geometry, but the phantom chambers that we used were cylindric. Nevertheless, our approach enabled us to eliminate potentially confounding factors such as geometry, tissue homogeneity, and measurement technique. In addition, three CT examinations were performed, and descriptive statistics were used to assess reproducibility; this statistical method is consistent with that in a previous phantom study of MR-measured section thickness (39).

For the chambers with simulated thicknesses of 0.25 and 0.50 mm, it was necessary to use a semiautomatic method to segment the simulated cartilage from the contrast-enhanced data sets. The reconstruction errors in the measurements of these chambers could have been influenced by user technique. However, the magnitude of the standard deviation error bars for thicknesses within this range was similar to that for thicknesses measured at nonenhanced CT, for which a purely automatic segmentation technique was used. Therefore, it appears that simulated cartilage reconstruction errors for thickness in this range would be high, regardless of the reconstruction technique used. Thus, caution should be exercised when making conclusions regarding thin cartilage (<0.75 mm in our phantom study).

The phantom was designed to simulate the interface between cartilage and cortical bone. There probably was some thinning of the polycarbonate at imaging due to volumetric averaging between the polycarbonate and the adjacent aluminum cylindric sleeve. However, the thickness of the aluminum sleeve wall was kept constant for each phantom cylinder, and the thresholding protocol was not biased toward changes between phantom chambers or whole data sets. Therefore, any errors introduced were consistent across all data sets, and, thus, simulated cortical bone was eliminated as a confounding factor.

From a basic science point of view, the following conclusion can be made: Since in our study errors were similar between the nonenhanced and contrast-enhanced (25% concentration) CT data sets, one can expect similar cartilage reconstruction errors when cadaveric tissues are CT scanned with or without contrast agent, assuming that a sufficient joint space is maintained and a low contrast agent concentration is used. However, given the additional technical challenges of keeping joint fluid within the capsule of a dissected joint, it seems more appropriate to scan the specimen without contrast agent.

In conclusion, the ability to reconstruct simulated cartilage by using a phantom and multidetector CT with and without arthrography is dependent on several factors, including contrast agent concentration, joint spacing, scanning direction, and spatial resolution. An improved understanding of the detection limits of multidetector CT cartilage reconstruction will assist in the diagnosis of joint abnormalities, interpretation of biomechanical models, and design of epidemiologic studies to investigate changes in cartilage thickness.

Practical applications: Our study results provide minimal boundaries for errors in multidetector CT measurements of cartilage thickness, as well as guidelines for practical use. It must be emphasized that the reported phantom reconstruction errors are probably best-case results since confounding factors were controlled. Higher contrast agent concentrations caused the simulated cartilage depicted on the CT images to appear thinner than the reference thickness; thus, use of a lower contrast agent concentration is likely to reduce the amount of volumetric averaging between actual cartilage and contrast agent. In addition, joint spacing should be maximized before CT scanning; this can be done by completely filling the joint capsule with diluted contrast solution and/or by applying traction to the joint. Failure to do this will result in increased errors when the width of the joint space reaches a critical threshold (0.5 mm in our phantom study). Finally, CT image reconstructions should be chosen such that isotropic or near-isotropic spatial resolution is achieved. Multidetector CT, unlike previous CT modalities, offers the ability to do this without increasing the radiation dose to the patient (40).

References

1. Vande Berg BC, Lecouvet FE, Poilvache P, et al. Assessment of knee cartilage in cadavers with dual-detector spiral CT arthrography and MR imaging. Radiology 2002;222:430–436.
2. Waldt S, Bruegel M, Ganter K, et al. Comparison of multislice CT arthrography and MR arthrography for the detection of articular cartilage lesions of the elbow. Eur Radiol 2005;15:784–791.
3. Schmid MR, Pfirrmann CW, Hodler J, Vienne P, Zanetti M. Cartilage lesions in the ankle joint: comparison of MR arthrography and CT arthrography. Skeletal Radiol 2003;32:259–265.
4. Nishii T, Tanaka H, Nakanishi K, Sugano N, Miki H, Yoshikawa H. Fat-suppressed 3D spoiled gradient-echo MRI and MDCT arthrography of articular cartilage in patients with hip dysplasia. AJR Am J Roentgenol 2005;185:379–385.
5. Daenen BR, Ferrara MA, Marcelis S, Dondelinger RF. Evaluation of patellar cartilage surface lesions: comparison of CT arthrography and fat-suppressed FLASH 3D MR imaging. Eur Radiol 1998;8:981–985.
6. El-Khoury GY, Alliman KJ, Lundberg HJ, Rudert MJ, Brown TD, Saltzman CL. Cartilage thickness in cadaveric ankles: measurement with double-contrast multi–detector row CT arthrography versus MR imaging. Radiology 2004;233:768–773.
7. Eckstein F, Stammberger T, Priebsch J, Englmeier KH, Reiser M. Effect of gradient and section orientation on quantitative analysis of knee joint cartilage. J Magn Reson Imaging 2000;11:469–470.
8. Eckstein F, Westhoff J, Sittek H, et al. In vivo reproducibility of three-dimensional cartilage volume and thickness measurements with MR imaging. AJR Am J Roentgenol 1998;170:593–597.
9. Sittek H, Eckstein F, Gavazzeni A, et al. Assessment of normal patellar cartilage volume and thickness using MRI: an analysis of currently available pulse sequences. Skeletal Radiol 1996;25:55–62.

10. Recht MP, Piraino DW, Paletta GA, Schils JP, Belhobek GH. Accuracy of fat-suppressed three-dimensional spoiled gradient-echo FLASH MR imaging in the detection of patellofemoral articular cartilage abnormalities. Radiology 1996;198:209–212.
11. Recht MP, Kramer J, Marcelis S, et al. Abnormalities of articular cartilage in the knee: analysis of available MR techniques. Radiology 1993;187:473–478.
12. Disler DG, McCauley TR, Kelman CG, et al. Fat-suppressed three-dimensional spoiled gradient-echo MR imaging of hyaline cartilage defects in the knee: comparison with standard MR imaging and arthroscopy. AJR Am J Roentgenol 1996;167:127–132.
13. Disler DG, McCauley TR, Wirth CR, Fuchs MD. Detection of knee hyaline cartilage defects using fat-suppressed three-dimensional spoiled gradient-echo MR imaging: comparison with standard MR imaging and correlation with arthroscopy. AJR Am J Roentgenol 1995;165:377–382.
14. Gold GE, Reeder SB, Yu H, et al. Articular cartilage of the knee: rapid three-dimensional MR imaging at 3.0 T with IDEAL balanced steady-state free precession—initial experience. Radiology 2006;240:546–551.
15. Gold GE, Hargreaves BA, Vasanawala SS, et al. Articular cartilage of the knee: evaluation with fluctuating equilibrium MR imaging—initial experience in healthy volunteers. Radiology 2006;238:712–718.
16. Eckstein F, Cicuttini F, Raynauld JP, Waterton JC, Peterfy C. Magnetic resonance imaging (MRI) of articular cartilage in knee osteoarthritis (OA): morphological assessment. Osteoarthritis Cartilage 2006;14(suppl A):A46–A75.
17. Cohen ZA, McCarthy DM, Kwak SD, et al. Knee cartilage topography, thickness, and contact areas from MRI: in-vitro calibration and in-vivo measurements. Osteoarthritis Cartilage 1999;7:95–109.
18. Eckstein F, Adam C, Sittek H, et al. Noninvasive determination of cartilage thickness throughout joint surfaces using magnetic resonance imaging. J Biomech 1997;30:285–289.
19. Haubner M, Eckstein F, Schnier M, et al. A non-invasive technique for 3-dimensional assessment of articular cartilage thickness based on MRI. II. Validation using CT arthrography. Magn Reson Imaging 1997;15:805–813.
20. Losch A, Eckstein F, Haubner M, Englmeier KH. A non-invasive technique for 3-dimensional assessment of articular cartilage thickness based on MRI. I. Development of a computational method. Magn Reson Imaging 1997;15:795–804.
21. McGibbon CA, Bencardino J, Yeh ED, Palmer WE. Accuracy of cartilage and subchondral bone spatial thickness distribution from MRI. J Magn Reson Imaging 2003;17:703–715.
22. Hardy PA, Nammalwar P, Kuo S. Measuring the thickness of articular cartilage from MR images. J Magn Reson Imaging 2001;13:120–126.
23. Eckstein F, Schnier M, Haubner M, et al. Accuracy of cartilage volume and thickness measurements with magnetic resonance imaging. Clin Orthop Relat Res 1998;352:137–148.
24. Wu JZ, Herzog W, Epstein M. Joint contact mechanics in the early stages of osteoarthritis. Med Eng Phys 2000;22:1–12.
25. Prevrhal S, Engelke K, Kalender WA. Accuracy limits for the determination of cortical width and density: the influence of object size and CT imaging parameters. Phys Med Biol 1999;44:751–764.
26. Prevrhal S, Fox JC, Shepherd JA, Genant HK. Accuracy of CT-based thickness measurement of thin structures: modeling of limited spatial resolution in all three dimensions. Med Phys 2003;30:1–8.
27. Nickoloff EL, Dutta AK, Lu ZF. Influence of phantom diameter, kVp and scan mode upon computed tomography dose index. Med Phys 2003;30:395–402.
28. Suzuki S, Yamamuro T, Okumura H, Yamamoto I. Quantitative computed tomography: comparative study using different scanners with two calibration phantoms. Br J Radiol 1991;64:1001–1006.
29. McPherson EJ, Friedman RJ, An YH, Chokesi R, Dooley RL. Anthropometric study of normal glenohumeral relationships. J Shoulder Elbow Surg 1997;6:105–112.
30. Mavcic B, Pompe B, Antolic V, Daniel M, Iglic A, Kralj-Iglic V. Mathematical estimation of stress distribution in normal and dysplastic hips. J Orthop Res 2002;20:1025–1030.
31. Takase K, Yamamoto K, Imakiire A, Burkhead WZ Jr. The radiographic study in the relationship of the glenohumeral joint. J Orthop Res 2004;22:298–305.
32. Ateshian GA, Soslowsky LJ, Mow VC. Quantitation of articular surface topography and cartilage thickness in knee joints using stereophotogrammetry. J Biomech 1991;24:761–776.
33. Shepherd DE, Seedhom BB. Thickness of human articular cartilage in joints of the lower limb. Ann Rheum Dis 1999;58:27–34.
34. Lorenson WE, Cline HE. Marching cubes: a high resolution 3D surface reconstruction algorithm. Comput Graph 1987;21:163–169.
35. Anderson AE, Peters CL, Tuttle BD, Weiss JA. Subject-specific finite element model of the pelvis: development, validation and sensitivity studies. J Biomech Eng 2005;127:364–373.
36. Chen SS, Falcovitz YH, Schneiderman R, Maroudas A, Sah RL. Depth-dependent compressive properties of normal aged human femoral head articular cartilage: relationship to fixed charge density. Osteoarthritis Cartilage 2001;9:561–569.
37. Huang CY, Stankiewicz A, Ateshian GA, Mow VC. Anisotropy, inhomogeneity, and tension-compression nonlinearity of human glenohumeral cartilage in finite deformation. J Biomech 2005;38:799–809.
38. Shepherd DE, Seedhom BB. The 'instantaneous' compressive modulus of human articular cartilage in joints of the lower limb. Rheumatology (Oxford) 1999;38:124–132.
39. Lemke AJ, Kazi I, de Bary P, et al. Development and evaluation of phantom for verification of section thickness at thin-section MR imaging. Radiology 2006;240:552–558.
40. Hsieh J. Image artifacts: appearances, causes and corrections. In: Hsieh J, ed. Proceedings of SPIE: computed tomography—principles, design, artifacts, and recent advances. Vol PM114. Bellingham, Wash: International Society for Optical Engineering, 2003; 167–240.

Radiology 2007

This is your reprint order form or pro forma invoice

(Please keep a copy of this document for your records.)

Reprint order forms and purchase orders or prepayments must be received 72 hours after receipt of form either by mail or by fax at 410-820-9765. It is the policy of Cadmus Reprints to issue one invoice per order. **Please print clearly**.

Author Name _____
Title of Article _____
Issue of Journal_____ Reprint # _____ Publication Date _____
Number of Pages_____ KB # _____ Symbol Radiology
Color in Article? Yes / No (Please Circle)

Please include the journal name and reprint number or manuscript number on your purchase order or other correspondence.

Order and Shipping Information

Reprint Costs (Please see page 2 of 2 for reprint costs/fees.)

_____ Number of reprints ordered $_____
_____ Number of color reprints ordered $_____
_____ Number of covers ordered $_____
Subtotal $_____
Taxes $_____

(*Add appropriate sales tax for Virginia, Maryland, Pennsylvania, and the District of Columbia or Canadian GST to the reprints if your order is to be shipped to these locations*.)

First address included, add $32 for each additional shipping address $_____

TOTAL $_____

Shipping Address (cannot ship to a P.O. Box) Please Print Clearly

Name _____
Institution _____
Street _____
City _____ State _____ Zip _____
Country _____
Quantity_____ Fax _____
Phone: Day _____ Evening _____
E-mail Address _____

Additional Shipping Address* (cannot ship to a P.O. Box)

Name _____
Institution _____
Street _____
City _____ State _____ Zip _____
Country _____
Quantity _____ Fax _____
Phone: Day _____ Evening _____
E-mail Address _____

** Add $32 for each additional shipping address*

Payment and Credit Card Details

Enclosed: Personal Check _____
Credit Card Payment Details _____
Checks must be paid in U.S. dollars and drawn on a U.S. Bank.

Credit Card: __ VISA __ Am. Exp. __ MasterCard
Card Number _____
Expiration Date_____
Signature: _____

Please send your order form and prepayment made payable to:

Cadmus Reprints
P.O. Box 751903
Charlotte, NC 28275-1903

Note: Do not send express packages to this location, PO Box.
FEIN #:541274108

Invoice or Credit Card Information

Invoice Address Please Print Clearly
Please complete Invoice address as it appears on credit card statement

Name _____
Institution _____
Department _____
Street _____
City _____ State _____ Zip _____
Country _____
Phone _____ Fax _____
E-mail Address _____

Cadmus will process credit cards and *Cadmus Journal Services* will appear on the credit card statement.

If you don't mail your order form, you may fax it to 410-820-9765 with your credit card information.

Signature _____ Date _____
Signature is required. By signing this form, the author agrees to accept the responsibility for the payment of reprints and/or all charges described in this document.

RB-9/22/06

Radiology 2007

Black and White Reprint Prices

Domestic (USA only)						
# of Pages	50	100	200	300	400	500
1-4	$213	$228	$260	$278	$295	$313
5-8	$338	$373	$420	$453	$495	$530
9-12	$450	$500	$575	$635	$693	$755
13-16	$555	$623	$728	$805	$888	$965
17-20	$673	$753	$883	$990	$1,085	$1,185
21-24	$785	$880	$1,040	$1,165	$1,285	$1,413
25-28	$895	$1,010	$1,208	$1,350	$1,498	$1,638
29-32	$1,008	$1,143	$1,363	$1,525	$1,698	$1,865
Covers	$95	$118	$218	$320	$428	$530

International (includes Canada and Mexico)						
# of Pages	50	100	200	300	400	500
1-4	$263	$275	$330	$385	$430	$485
5-8	$415	$443	$555	$650	$753	$850
9-12	$563	$608	$773	$930	$1,070	$1,228
13-16	$698	$760	$988	$1,185	$1,388	$1,585
17-20	$848	$925	$1,203	$1,463	$1,705	$1,950
21-24	$985	$1,080	$1,420	$1,725	$2,025	$2,325
25-28	$1,135	$1,248	$1,640	$1,990	$2,350	$2,698
29-32	$1,273	$1,403	$1,863	$2,265	$2,673	$3,075
Covers	$148	$168	$308	$463	$615	$768

Minimum order is 50 copies. For orders larger than 500 copies, please consult Cadmus Reprints at 800-407-9190.

Reprint Cover

Cover prices are listed above. The cover will include the publication title, article title, and author name in black.

Shipping

Shipping costs are included in the reprint prices. Domestic orders are shipped via UPS Ground service. Foreign orders are shipped via a proof of delivery air service.

Multiple Shipments

Orders can be shipped to more than one location. Please be aware that it will cost $32 for each additional location.

Delivery

Your order will be shipped within 2 weeks of the journal print date. Allow extra time for delivery.

Color Reprint Prices

Domestic (USA only)						
# of Pages	50	100	200	300	400	500
1-4	$218	$233	$343	$460	$579	$697
5-8	$343	$388	$584	$825	$1,069	$1,311
9-12	$471	$503	$828	$1,196	$1,563	$1,935
13-16	$601	$633	$1,073	$1,562	$2,058	$2,547
17-20	$738	$767	$1,319	$1,940	$2,550	$3,164
21-24	$872	$899	$1,564	$2,308	$3,045	$3,790
25-28	$1,004	$1,035	$1,820	$2,678	$3,545	$4,403
29-32	$1,140	$1,173	$2,063	$3,048	$4,040	$5,028
Covers	$95	$118	$218	$320	$428	$530

International (includes Canada and Mexico))						
# of Pages	50	100	200	300	400	500
1-4	$268	$280	$412	$568	$715	$871
5-8	$419	$457	$720	$1,022	$1,328	$1,633
9-12	$583	$610	$1,025	$1,492	$1,941	$2,407
13-16	$742	$770	$1,333	$1,943	$2,556	$3,167
17-20	$913	$941	$1,641	$2,412	$3,169	$3,929
21-24	$1,072	$1,100	$1,946	$2,867	$3,785	$4,703
25-28	$1,246	$1,274	$2,254	$3,318	$4,398	$5,463
29-32	$1,405	$1,433	$2,561	$3,788	$5,014	$6,237
Covers	$148	$168	$308	$463	$615	$768

Tax Due

Residents of Virginia, Maryland, Pennsylvania, and the District of Columbia are required to add the appropriate sales tax to each reprint order. For orders shipped to Canada, please add 7% Canadian GST unless exemption is claimed.

Ordering

Reprint order forms and purchase order or prepayment is required to process your order. Please reference journal name and reprint number or manuscript number on any correspondence. You may use the reverse side of this form as a proforma invoice. Please return your order form and prepayment to:

Cadmus Reprints
P.O. Box 751903
Charlotte, NC 28275-1903

Note: Do not send express packages to this location, PO Box.
FEIN #:541274108

Please direct all inquiries to:

Rose A. Baynard
800-407-9190 (toll free number)
410-819-3966 (direct number)
410-820-9765 (FAX number)
baynardr@cadmus.com (e-mail)

Reprint Order Forms and purchase order or prepayments must be received 72 hours after receipt of form.